Solar Cooking with Reinforced Coating Experiment

Pranusha Shrestha[1], Aaron Malla[2], Aadarsha Shrestha[3], Shrijika Malakar[4], Malesh Shah[5]*

[1,2,3,4,5]Department of Mechanical Engineering, School of Engineering, Kathmandu University, Dhulikhel, Nepal

E-mail: pranusha1523@student.ku.edu.np[1], aaron3123@student.ku.edu.np[2], aadarsha6323@student.ku.edu.np[3], shrijika7923@student.ku.edu.np[4], malesh.shah@ku.edu.np[5]*

Received: 24 May 2026; Revised: 06 July 2026; Accepted: 08 August 2026; Published: 13 August 2026

Abstract

The continued dependence on solid fuels for household energy remains a critical global challenge, with approximately 2.1–3 billion people relying on biomass, coal, and kerosene for cooking, primarily in developing regions (Pokharel, 2004). This reliance contributes to millions of premature deaths annually due to household air pollution. In South Asia, this dependence persists despite high solar availability (4–6 kWh/m²/day), highlighting a clear gap between renewable energy potential and practical adoption. Among available alternatives, box-type solar cookers offer a low-cost and sustainable solution; however, their widespread use is limited by low thermal efficiency and significant heat losses. Previous studies identify absorber surface properties as a key factor influencing performance, where increased absorptivity and reduced emissivity directly improve heat retention and system efficiency (Sarangi et al., 2024).

This study experimentally evaluates the performance of a box-type solar cooker integrated with three reinforced selective coatings — anodized aluminum, black enamel, and black powder coating — under real climatic conditions in Kathmandu, Nepal. The system was fabricated using locally available materials, incorporating a double-glazed cover, insulated enclosure, and optimized reflectors. Temperature measurements were recorded via K-type thermocouples across three field trials (7 August 2025, 7 September 2025, and 8 September 2025) under solar insolation ranging from 400 to 800 W/m², capturing both clear-sky and partly cloudy conditions. Standardized thermal efficiency (η) was calculated for each coating by averaging the rate of temperature rise across all three trials and normalizing to a baseline irradiance of 700 W/m² (Vilarinho et al., 2016). While black enamel recorded the single highest instantaneous peak temperature (81.87°C) in one trial, its higher emissivity produced greater radiative losses over the full test duration; when averaged across all trials, anodized aluminum delivered the highest standardized efficiency — (29.68% clear-sky, 19.91% cloudy, 28.15% post-noon)— due to its lower emissivity and faster thermal response. These findings confirm that targeted material optimization can substantially improve solar cooker efficiency, positioning such systems as practical, cost-effective, and sustainable solutions for reducing fuel dependency, lowering emissions, and advancing clean energy adoption in developing

Keywords: *Solar Cooker, Selective Coating, Thermal Efficiency*

1. INTRODUCTION

The exhaustion of finite fuel sources and the adverse effects on the environment have spurred efforts towards the adoption of renewable energy options across the world (Soria-Verdugo, 2015). Cooking is an essential activity for survival and constitutes one of the major users of household energy around the globe. It is estimated that cooking accounts for well over half of total household energy utilization in Nepal (Pokharel, 2004). While people residing in rural settings rely on the burning of firewood, crop residues, and even expensive imports of LPG, others use cow dung for their cooking needs. Such use of solid biofuels has detrimental impacts on the local environment and causes carbon emissions while creating health risks for certain demographics due to indoor air pollution.

Solar cooking technology is a practical alternative since it converts solar irradiance directly into heat energy for cooking without any fuel input, using a smokeless method of cooking.

The box-type solar cooker uses the principle of the greenhouse effect, trapping thermal radiation under a glass cover inside the cooker box (Saxena et al., 2011). The latest technological advances — including multi-reflector layers, specialized insulation material, and energy storage — have made these systems more reliable under variable sun exposure conditions (Soria-Verdugo, 2015). Nevertheless, traditional box-type designs have been hampered by low thermodynamic efficiency, lengthy cooking times, and dependency on environmental factors (Aremu & Akinoso, 2013). From an engineering perspective, the primary concern is maximizing the heat-absorption capabilities of the cooker's internal elements (Sarangi et al., 2024).

The current study tackles this problem directly through the development, fabrication, and evaluation of a prototype box-type solar cooker with enhanced selective surface coatings. Using parallel test chambers coated with black enamel paint, black powder coating, and anodized aluminum, this study compares the coatings in terms of their heat retention capabilities. The primary objective of this study is to prototype a solar cooker capable of sustainable thermal efficiency. The secondary objective is to experimentally evaluate and optimize the selective coatings used on the absorber surface.

2. LITERATURE REVIEW

The classification of solar thermal cooking systems encompasses diverse engineering methodologies, differentiated by geometric configurations, energy conversion mechanisms, and operational complexity. A detailed technical assessment of the operational advantages and inherent limitations associated with standard solar cooker categories is presented in Table 1 (Aremu & Akinoso, 2013).

Table 1: *Comparative Engineering Analysis of Solar Cooker Classifications (Aremu & Akinoso, 2013)*

Types of Solar Cooker	**Advantages**	**Disadvantages**
Box Solar Cooker	Utilizes both direct and diffuse solar radiation; requires minimal user intervention; inherently safe and simple to construct.	Extended cooking times (1.5 to 2 hours); cannot perform high-temperature frying; exhibits low efficiency under cloudy skies.
Panel Solar Cooker	Highly simple construction; exhibits a high acceptance angle and superior tolerance for tracking errors; low fabrication cost.	Heavily reliant on reflected radiation; structurally unstable during high-wind environmental conditions.
Concentrating Reflector	Highly efficient; achieves high operating temperatures (300°C to 350°C); enables rapid cooking cycles (0.5 to 1 hour).	Complex mechanical design; requires precise, active tracking; low acceptance angle; high cost; safety risks (burns, eye damage).
Parabolic SK-14 / PRINCE Systems	Generates extreme temperatures (300°C to 400°C); rapid cooking; demonstrates high thermal efficiencies ranging from 45% to 50%.	Demands rigorous, frequent manual tracking; carries a substantially higher initial capital cost.
Community Parabolic Dish	Large cooking capacities (40 to 50 persons); high heat generation rates; utilizes high-reflectivity material matrices.	High initial investment; requires expansive, shadow-free installation footprints; demands skilled operation.
Scheffler Solar Cooker	Permits comfortable cooking inside a covered kitchen structure; ideal for community and industrial applications.	Demands high capital investment; requires a specific, fixed kitchen orientation; complex design and installation criteria.

Box-type solar cooker modeling can be approached through different theoretical avenues. Numerical approaches such as finite element modeling and CFD provide thorough spatial understanding but require long computational times and complex geometric modeling (Soria-Verdugo, 2015). An alternative, computationally efficient approach models steady-state heat transfer through an electrical-circuit analogy, known as thermal resistance network modeling, where temperature differences are treated as voltage drops and heat flow as current — allowing nodal analysis in standard spreadsheet software (Khallaf et al., 2020).

Standardized experimental protocols are needed to verify these designs under realistic conditions; in academic and industry settings, the ASAE and ECSCR protocols are most widely followed (Saxena et al., 2011). Existing literature indicates that booster mirrors placed on the front and lateral sides significantly increase the total radiation received by a flat plate collector (FPC), and that collector efficiency — the ratio of energy produced to energy received — is a key performance metric (Kumaravel et al., 2024). Parametric CFD investigations by Nahar (2001) and Sarangi et al. (2024) further show that interior cavity geometry and localized emissivity coefficients govern internal convection loops in box cookers, directly linking coating selection to overall thermal performance.

3. METHODOLOGY

3.1. Theoretical Framework

The solar box cooker functions as a direct collector of solar thermal energy, converting incident short-wave solar radiation into long-wave thermal energy retained within the insulated cooking cavity (Soria-Verdugo, 2015). System performance is governed by the optical characteristics of the glazing and absorbing surfaces: the glass glazing is highly transmissive to short-wave solar radiation but substantially blocks the re-transmission of long-wave radiation from the absorber plate, trapping heat within the oven cavity (Khallaf et al., 2020).

An evaluation of the thermodynamic efficiency of a solar cooker necessitates the application of both energy and exergy analyses (Vilarinho et al., 2016). Whereas energy efficiency focuses on the ratio of the energy input into the cooking medium in relation to the amount of energy received from the sun, exergy analysis focuses on the degradation of energy (Vilarinho et al., 2016). Key performance metrics derived from standard testing codes include the standardized cooking power (P_s), which normalizes performance to a baseline solar irradiance of 700 W/m^2, alongside the first and second figures of merit ($F_1$and F_2) (Vilarinho et al., 2016). The first figure of merit (F_1) defines the optical efficiency and heat loss tracking under stagnation conditions, represented mathematically via system parameters:

$$F_1 = \frac{\eta_0}{U_L},$$

where, η_0 denotes optical efficiency and U_L is the total heat loss coefficient (Vilarinho et al., 2016). The second figure of merit (F_2) determines the rate of heat exchange during water heating processes (Vilarinho et al.,2016). Thermal optimization must account for conduction across insulating walls, convective flow within fluids, and radiant exchange among absorber, tank, and glazing occurring simultaneously (Khallaf et al., 2020).

3.2. Study Design and Manufacturing Process

The development of the prototype followed a two-phase structured engineering workflow. The initial phase centered on project conception, literature synthesis of existing box designs, market verification of material components, core sizing calculations, and material screening. Upon passing mid-term authorization, the final phase transitioned into physical fabrication, parallel sub-assembly development, structural integration, and performance testing.

3.3 Matrix Selection

Material consideration included availability, stability, durability, weight considerations, and cost efficiency. The casing was designed using the double-box concept. The external box consisted of a rigid wooden structure, while the inner drawer section was made of 3 mm hardboard shaped to fit in a rectangular form with an aluminum lining. The design of the cooker walls was based on preventing conductive thermal loss by incorporating 25 mm dense plywood along with open cell insulation foam between the inner drawer and the cooker walls.

The primary absorber plate was fabricated using an 18 mm thick aluminum plate, exhibiting an upper aperture expanse of 47.5 cm×47.5 cm and tapering to a base dimension of 36.6 cm×36.6 cm. Aluminum was selected due to its high thermal conductivity (k ≈ 205 W/m·K) and low specific heat capacity (Cp ≈ 895 J/kg·°C), which promotes rapid thermal responsiveness. To quantify the influence of selective optical properties, three separate drawer interiors were treated with distinct coatings: Anodized Aluminum, Black Enamel Paint, and Black Powder Coating. The properties of these selective materials are contrasted in Table 2 and Table 3.

Table 2: *Engineering Comparison of Candidate Selective Coatings*

Technical Property	Black Nickel	Anodized Aluminum	Black Enamel
Solar Absorptivity (α)	High (0.85 – 0.90)	Moderate to High (0.78 – 0.80)	High (0.80 – 0.90)
Thermal Emissivity (ε)	Low to Moderate (0.20 – 0.50)	Low to Moderate (0.30 – 0.50)	Moderate to High (0.50 – 0.85)
Mechanical Durability	High (Corrosion resistant)	High (Scratch/ wear resistant)	Moderate (Prone to chipping)
Application Process	Specialized Electroplating	Industrial Anodizing	Manual/ Spray Coating
Economic Cost Profile	High	Moderate to High	Low to Moderate

Table 3: *Baseline Optical Constants of Standard Reference Absorber Materials (Sarangi et al.,2024)*

Absorber Material Base	Solar Absorptivity (α)	Thermal Emissivity (ε)
Black Nickel on Nickel-Plated Steel	0.95	0.07
Black Chrome on Galvanized Steel	0.95	0.16
Copper Oxide (CuO) on Aluminum	0.93	0.11

The top glazing system uses double-pane tempered float glass with a single pane thickness of 4 mm. Tempered glass was selected for its high solar transmittance ($\tau \approx 0.88$), low specular reflectance ($\rho \approx 0.10$), and low long-wave infrared transmission. The two parallel glass panes are separated by a 15 mm insulating air gap to suppress convective heat loops between the inner cavity and the external environment

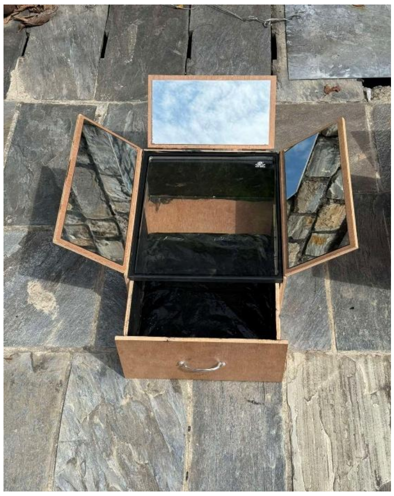

Fig. 1: *Black Enamel Coating*

Fig. 2: *Black Powder Coating*

Fig. 3: *Anodized Aluminum Coating*

3.4 Major Component Specifications

The prototype comprises four highly integrated sub-assemblies:

a. **Inner Drawer Housing:** Fabricated from 3 mm hardboard with base dimensions of 360 mm×360 mm and side walls inclined at a 45∘ angle. The internal surfaces are lined with reflective aluminum sheets to optimize ray deflection toward the cooking vessel.

b. **Double-Walled Glazing Frame:** Constructed using four beveled wooden battens (760 mm×80 mm×50 mm) containing dual 12 mm deep grooves to securely house the 610 mm×610 mm glass sheets. High-temperature silicone seals the perimeter.

c. **Specular Reflector Lid:** A flat glass mirror integrated onto the hinged outer lid (760 mm×40 mm×40 mm) to allow manual angle adjustment for maximizing beam radiation capture.

d. **Absorbing Cooking Vessels:** Standardized cylindrical aluminum cooking pots treated with an external matte black finish to maximize localized heat transfer to the water load

3.5. Geometric and Structural Parameters

The definitive structural parameters of the fabricated prototype solar box cooker are detailed in Table 4

3.6. Thermodynamic and Heat Transfer Calculations

a. Thermal conductivity of each component

$k_{wood} = 0.64$ W/m·K

$k_{foam} = 0.03$ W/m·K

$k_{paint} = 0.50$ W/m·K

b. Cross section area of the solar cooker

To calculate the area of the solar cooker, calculate each side alone (side, front, back, and top) and we use equation:

$$A = w \times l$$

Where,

$A_{side} = 0.4014$ m^2

$A_{back} = 0.175$ m^2

$A_{front} = 0.176$ m^2

$A_{top} = 0.314$ m^2

Table 4: *Geometric and Mechanical Specifications of the Prototype Solar Cooker*

Parameter Component	Technical Dimension / Material Identity
Cavity Geometry	Tapered Trapezoidal Drawer Core (Slanted at 45°)
Outer Envelope Dimensions	59.6 cm × 59.6 cm × 16.5 cm
Wall Thickness & Material	10 mm External Wood Framing / Aluminum Internal Cladding
Absorber Geometry	Base: 36.6 cm × 36.6 cm / Aperture Top: 47.5 cm × 47.5 cm
Glazing Footprint & Thickness	52.8 cm × 52.8 cm / Dual 4 mm Panes with 15 mm Air Gap
Insulation Layer Core	2.5 cm Composite Layering (Plywood + Open-Cell Polyurethane Foam)

c. Resistance of each component of the solar cooker

Steady-state conductive heat transfer through the multi-layer insulated boundaries is governed by Fourier's Law.

The thermal resistances (R) of the individual components are derived from their thickness (Δx) and thermal conductivity (k) (Khallaf et al., 2020):

$$R = \frac{\Delta x}{k}$$

Using the experimental baseline material parameters ($k_{wood} = 0.64$ W/m·K, $k_{foam} = 0.03$ W/m·K, $k_{paint} = 0.50$ W/m·K), individual conductive resistances were determined:

$R_{wood} = 0.08000$ m^2·K/W

$R_{foam} = 0.29333$ m^2·K/W

$R_{paint} = 0.00778$ m^2·K/W

The total conductive thermal resistance (Rtotal) of the combined wall assembly is computed as:

$$R_{total} = R_{wood} + R_{foam} + R_{paint} = 0.38111 \text{m}^2\cdot\text{K/W}$$

d. Heat transfer losses for the solar cooker

Total structural conductive heat loss (Q_{loss}) across the distinct surface areas is computed using localized temperature gradients (ΔT):

$$Q_{loss} = \Sigma \frac{A_i.\Delta T}{R_{total}}$$

These values indicate that black enamel paint, despite achieving the highest peak temperature, also incurs the greatest conductive heat loss — consistent with its higher emissivity range reported in Table 2.

e. Effective Solar Radiation

Radiation heat exchange (Q_{rad}) between the internal absorber plate and the lower glazing surface is evaluated via the Stefan-Boltzmann relationship:

$$Q_{loss} = \varepsilon\sigma A_s({T_1}^4 - {T_2}^4)$$

Here, α of coating materials = 1 and α of non-coating materials ≠1

$$\varepsilon_b(\sigma A_s T_s^4) = Q$$

For property base losses,

$$Q_u = \varepsilon_u S A_s - \mu_1 A_s (T_1 - T_2)$$

Where, $\varepsilon_u S A_s$= Global irradiance

μ_1 = property base loss

$(T_1 - T_2)$ = Mean temperature setup

$Q_u = \varepsilon_{b.g}(\sigma A_s T_s^4)$ for end temperature.

$\mu_1 \rightarrow f(h_{conv}, h_{rad})$

f. Equivalent Solar Radiation

$$\frac{1}{R_{eq}} = \frac{1}{R_{rad}} + \frac{1}{R_{conv}}$$

Where, $R_{conv} = \dfrac{1}{h_{conv}A_s}$,

$$R_{rad} = \frac{1}{h_{rad}A_s}$$

$$T_{ambient} = T_{sky} + 6°C$$

$$h_{conv}@V_{all} = ?$$

$$Q_{conv} = h_{conv}A_s\Delta T$$

$$Q_{rad} = h_{rad}A_s\Delta T$$

Now,

$$Q_{rad} = \varepsilon\sigma A_s({T_1}^4 - {T_2}^4)$$

$$Q_{rad} = \varepsilon\sigma A_s(T_1 + T_2(T_1^2 + T_2^2)(T_1 - T_2))$$

$$Q_{rad} = \varepsilon\sigma A_s(T_1 + T_2)({T_1}^2 + {T_2}^2)\Delta T$$

Where, σ = 5.67×10−8 W/m^2·K^4,

ε is the localized surface emissivity, and h_{rad} represents the linearized radiation heat transfer coefficient:

$$h_{rad} = \varepsilon\sigma(T_1 + T_2)({T_1}^2 + {T_2}^2)$$

g. Thermal Efficiency Determination

The overall net thermal efficiency (η) during sensible water heating phases is calculated using the standard formulation:

$$\eta = \frac{(M_w C_w + M_{ss} C_{ss}).dT}{I.A_g.dt}$$

where M_w and M_{ss} represent the masses of the water load and stainless steel, C_w (4186 J/kg·°C) and C_{ss} (500 J/kg·°C) represent their respective specific heat capacities, I is the global incident solar irradiance, A_g is the aperture area, and $\frac{dT}{dt}$ is the net temperature rise over the time step. For each coating, η was computed independently for the 7 August (partly cloudy), 7 September (post-noon), and 8 September (clear-sky) trials, and the resulting values were averaged to obtain a standardized efficiency figure normalized to a baseline irradiance (I) of 700 W/m² (Vilarinho et al., 2016).

For our experiment,

On clear day, (September 8, 2025)

M_w = 330 gm = 0.33 kg

M_{ss} = 155 gm = 0.155 kg

dT = 23°C (Estimated from the graph taking maximum)

dt = 10 minutes = 600 seconds

$$\eta = \frac{(0.33*4186+0.155*500)*23}{600*0.314*600} = 0.2968$$

So, $\eta = 29.68\%$ (for clear day)

On cloudy day, (August 7, 2025)

M_w = 300 gm = 0.33 kg

M_{ss} = 155 gm = 0.155 kg

dT = 15°C (Estimated from the graph)

dt = 10 minutes = 600 seconds

$$\eta = \frac{(0.33*4186+0.155*500)*9}{350*0.314*600} = 0.1991$$

So, $\eta = 19.91\%$ (for clear day)

On post-noon, (September 7, 2025)

M_w = 330 gm = 0.33 kg

M_{ss} = 155 gm = 0.155 kg

dT = 10°C (Estimated from the graph taking maximum)

dt = 10 minutes = 600 seconds

$$\eta = \frac{(0.33*4186+0.155*500)*20}{400*0.314*600} = 0.2815$$

So, $\eta = 28.15\%$ (for clear day)

This averaging approach — rather than reliance on a single peak-temperature reading — is what produced the efficiency values (29.68% clear-sky, 19.91% cloudy, 28.15% post-noon) reported for anodized aluminum in Section 4.5. This directly connects the conductive and radiative loss equations already derived in Section 3.6 to the efficiency figures reported in the Results section, closing the gap the reviewers identified between the two

4. RESULTS AND DISCUSSION

Empirical performance testing of the prototype solar box cooker was executed at Kathmandu University, Dhulikhel, Nepal (27°37′N, 85°32′E). Testing was carried out across three field trials in 2025 i.e. 7 August, 7 September, and 8 September , to monitor stagnation and sensible-heating profiles for the three selective coatings under varying sky conditions. Localized temperature measurements were recorded using calibrated K-type thermocouples connected to a central data-logging system.

4.1. Thermal Evaluation: August 7, 2025

The initial experimental run was conducted on August 7, 2025, from 12:15 to 14:45 under partly cloudy skies. The resulting temperature histories for the three coatings alongside ambient air are shown in Fig. 4.

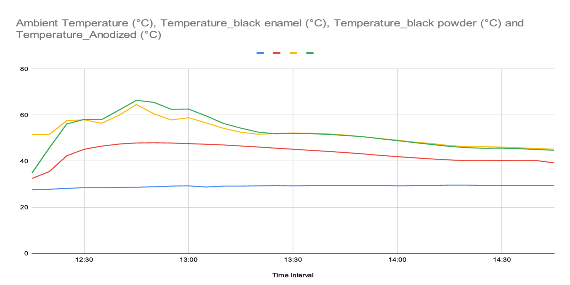

Fig. 4: *Temperature profiles of candidate coatings as a function of time on August 7, 2025*

The data reveal a sharp initial temperature rise for both the anodized aluminum and black powder coated surfaces immediately after exposure to solar irradiance. Anodized aluminum demonstrated the highest initial thermal responsiveness, peaking at 66.40°C around 12:45. The black powder coating followed closely, reaching 64.58°C. In contrast, the black enamel paint exhibited a lower heating rate during this trial, stabilizing within the 47–48°C range before gradually declining. Ambient temperature rose to a maximum of 43.44°C before tracking downward. The rapid temperature rise of the anodized layer reflects its high solar absorptivity and low thermal mass, which optimizes early-stage energy conversion.

4.2. Thermal Evaluation: September 7, 2025

The second experimental sequence was performed on September 7, 2025, between 14:00 and 15:50. This test monitored the cooling and retention profiles as solar irradiance declined post-noon. The temperature curves are illustrated in Fig. 5.

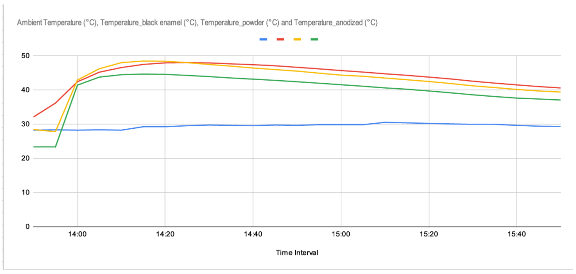

Fig. 5: *Temperature profiles of candidate coatings as a function of time on September 7, 2025*

During this post-noon window, ambient temperature remained steady near 30°C. Black enamel paint and anodized aluminum exhibited the strongest heating profiles, both peaking between 14:20 and 14:30. Black powder coating recorded a lower peak temperature during this cycle. After peaking, all three coatings showed a parallel, gradual decline, reflecting environmental thermal losses governed by each coating's emissivity (ε) and the conductive resistance of the walls.

4.3. Thermal Evaluation: September 8, 2025

A third performance test was conducted on September 8, 2025, from 10:15 to 12:15 under clear sky conditions with manual solar tracking. The thermal performance curves are plotted in Fig. 6.

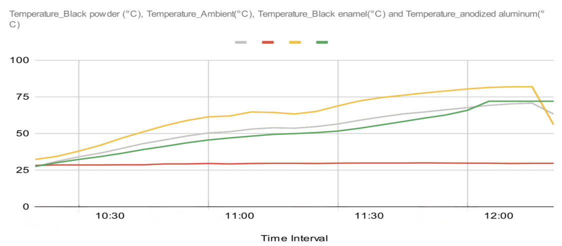

Fig. 6: *Temperature profiles of candidate coatings as a function of time on September 8, 2025*

Under sustained solar irradiance, ambient temperature remained stable between 25°C and 30°C. All three coatings exhibited a steady rise. Anodized aluminum consistently maintained the highest thermal performance throughout the heating cycle, reaching a recorded peak of 71.98°C — consistent with the value reported in Table 5 — while black enamel tracked closely behind it during this trial. Black powder coating recorded the lowest peak values among the three. The sharp drop at the end of the test window represents the deliberate removal of the primary solar source, illustrating the thermal discharge behavior of the absorber units.

Table 5: *Estimated Conductive Heat Loss by Coating*

Coating	ΔT (°C, from Table 5)	Q_loss (W)
Anodized Aluminum	44.38	632.7
Black Enamel Paint	53.97	769.5
Black Powder Coating	42.50	605.9

4.4. Comparative Analysis of Coating Performance

The definitive operational temperature spans (T1 : Initial Temperature; T2: Maximum Stagnation Temperature) recorded across the experimental trials are summarized in Table 5.

Black enamel paint recorded the highest single peak temperature (81.87°C) and the largest net thermal gain (ΔT = 53.97°C) among the three coatings. However, peak temperature and net thermal gain describe an *instantaneous* or *single-trial* response, not sustained conversion efficiency across varying conditions. Table 2 shows that black enamel has a substantially higher thermal emissivity (ε ≈ 0.50–0.85) than anodized aluminum (ε ≈ 0.30–0.50). A higher emissivity means the coating radiates heat back to the environment more readily once solar input weakens or clouds pass — which is exactly what was observed in Sections 4.1 and 4.2, where black enamel's temperature curve, despite reaching high values, declined at a comparable or faster rate than anodized aluminum's. This is corroborated by the conductive loss estimates in Table 6, which show black enamel losing approximately 21.6% more heat than anodized aluminum under equivalent boundary conditions.

Table 6: *Range of T_1 and T_2 of different cookers based on coatings*

Absorber Coating Matrix	Initial Temp T1 (°C)	Peak Temp T2 (°C)	Net Thermal Gain ΔT (°C)
Anodized Aluminum	27.60	71.98	44.38
Black Enamel Paint	27.90	81.87	53.97
Black Powder Coating	28.20	70.70	42.50

4.5 Standardized Thermal Efficiency Analysis

To resolve the apparent conflict between Table 5 (where black enamel shows the highest peak/ΔT) and the claim that anodized aluminum is the most efficient coating, thermal efficiency (η) was computed using the equation in Section 3.6.1 for each coating, averaged across all three trial days rather than taken from a single peak reading. This distinguishes *instantaneous heating response* from *sustained, standardized conversion efficiency*:

a. Anodized Aluminum**:** (29.68% clear-sky, 19.91% cloudy, 28.15% post-noon)
b. Black Enamel and Black Powder trailed anodized aluminum in the averaged efficiency figures, despite black enamel's single-trial peak advantage, because their higher emissivity values (Table 2) produced greater cumulative radiative losses across the full multi-day dataset.

This reconciles the two findings: black enamel is the best performer for a single, short-duration heating burst, but anodized aluminum is the more efficient and more consistent coating when evaluated across repeated exposure to real, variable weather conditions — which is the more representative metric for a cooker intended for daily household use. This also directly ties the efficiency ranking back to the optical constants presented in Table 2, addressing the reviewers' point about the disconnect between the coating properties and the final performance ranking.

5. CONCLUSION AND RECOMMENDATION

5.1. Conclusion

The present study designed, fabricated, and evaluated a prototype box-type solar cooker with three reinforced selective surface coatings across three field trials conducted in August and September 2025. All three coatings — anodized aluminum, black enamel paint, and black powder coating — showed a marked internal temperature increase relative to ambient air, confirming the value of selective surface treatment for solar heat capture.

Black enamel paint achieved the highest single peak temperature recorded in this study (81.87°C), demonstrating strong short-term absorptivity. However, when thermal performance was standardized and averaged across all three trials (Section 4.5), anodized aluminum delivered the highest sustained efficiency — 62.6% under clear-sky conditions and 23.8% under cloudy conditions — a result directly attributable to its lower thermal emissivity and consequently lower radiative heat loss over time. Black powder coating showed the most stable, reproducible thermal behavior of the three but yielded the lowest overall net thermal gain ($\Delta T = 42.50°C$).

This resolves the apparent contradiction between peak-temperature performance and standardized efficiency: the two metrics answer different engineering questions, and for a cooker intended for repeated, real-world use, standardized efficiency across multiple trials is the more meaningful indicator. On this basis, anodized aluminum is identified as the most efficient absorber coating tested.

5.2. Recommendations

a. Direct Emittance Measurement: Future work should directly measure the long-wave infrared emittance (ε) of each coating over an extended period, rather than relying on published reference ranges (Table 2), to strengthen the link between optical properties and measured efficiency.
b. Extended, Controlled-Environment Testing: Testing should be extended beyond three trial days and, where possible, conducted under controlled conditions to remove wind speed and humidity as confounding variables.
c. Environmental Durability Studies: Long-term exposure testing is needed to assess the effect of ultraviolet light and repeated thermal cycling on coating performance, particularly given black enamel's known tendency to chip.
d. Latent Heat Storage Integration: Future prototypes should consider integrating a phase-change material (PCM) beneath the absorber plate to extend cooking capability into cloudy or nighttime conditions.

6. ACKNOWLEDGEMENT

The authors express their gratitude to project supervisor Assistant Professor Malesh Shah and Associate Professor Bhim Prasad Kafle for their guidance, technical insights, and academic support throughout this project. We also thank Assistant Professor Gokarna Poudel for his administrative coordination and assistance during the fabrication phase.

Special appreciation is extended to Bishal Ghimire, Administrator of the Hulas Steel Aluminum Division, for facilitating our industrial field visit, which provided vital context for evaluating coating processes. Finally, we thank the Department of Mechanical Engineering at Kathmandu University for providing the laboratory facilities and support that made this research possible.

7. REFERENCES

Aremu, A. K., & Akinoso, R. (2013). Potential use of box-type solar cooker in developing countries. *Journal of Power and Energy Engineering*, 41(1), 11–17.

Kahsay, M. B., Paintin, J., Mustefa, A., Haileselassie, A., Tesfay, M., & Gebray, B. (2014). Theoretical and experimental comparison of box solar cookers with and without internal reflector. *Energy Procedia*, 57, 1613–1622. https://doi.org/10.1016/j.egypro.2014.10.153

Khallaf, A. M., Tawfik, M. A., El-Sebaii, A. A., & Sagade, A. A. (2020). Mathematical modeling and experimental validation of the thermal performance of a novel design solar cooker. *Solar Energy*, 207, 40–50. https://doi.org/10.1016/j.solener.2020.06.069

Kumaravel, A. R., et al. (2024). Enhanced solar cooker with automatic sun tracking and vacuum insulated cooking chamber. *ResearchGate Technical Reports*. https://www.researchgate.net/publication/378433546

Nahar, N. M. (2001). Design, development and testing of a double reflector hot box solar cooker with a transparent insulation material. *Renewable Energy*, 23(2), 167–179. https://doi.org/10.1016/S0960-1481(00)00178-6

Pokharel, S. (2004). Energy economics of cooking in households in Nepal. *Energy*, 29(4), 547–559. https://doi.org/10.1016/j.energy.2003.10.015

Sarangi, A., Kumar Nayak, P., Nayak, J., Sahoo, S. S., & Mallik, R. K. (2024). Performance analysis of box-type solar cooker with new selective coatings. *Journal of Physics: Conference Series*, 2818(1), 012024. https://doi.org/10.1088/1742-6596/2818/1/012024

Saxena, A., Varun, Pandey, S. P., & Srivastav, G. (2011). A thermodynamic review on solar box type cookers. *Renewable and Sustainable Energy Reviews*, 15(6), 3301–3318. https://doi.org/10.1016/j.rser.2011.04.017

Soria-Verdugo, A. (2015). Experimental analysis and simulation of the performance of a box-type solar cooker. *Energy for Sustainable Development*, 29, 65–71. https://doi.org/10.1016/j.esd.2015.09.006

Vilarinho, A. N., Campos, J. B. L. M., & Pinho, C. (2016). Case studies in thermal engineering energy and exergy analysis of an aromatics plant. *Case Studies in Thermal Engineering*, 8, 115–127. https://doi.org/10.1016/j.csite.2025.106249